Construction and Building Materials 393 (2023) 132123

Contents lists available at ScienceDirect

Construction and Building Materials

journal homepage: www.elsevier.com/locate/conbuildmat

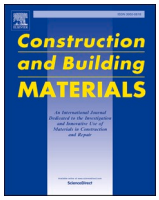

Effect of high temperature on textile reinforced Mortar-to-masonry bond

L. Estevan *, F.J. Baeza, F.B. Varona, J. Pereiro

Department of Civil Engineering, University of Alicante, P.O. Box 99, 03080 Alicante, Spain

ARTICLE INFO

Keywords:
TRM
FRCM
Masonry
Bond
High temperature

ABSTRACT

One of the most important factors that define the effectiveness of Textile Reinforced Mortar (TRM) is their bond capacity to the substrate. This property may be compromised in case of exposure to high temperatures, although the information available on this topic is very limited at the moment. This paper analyzes the bond behavior on clay brick substrates of TRMs with carbon or glass textiles and different hydraulic lime mortar matrix. The effect of bond length and 3 levels of exposure temperature (20, 200 and 400 °C) are studied. The results show that at 200 °C the TRMs analyzed retain a significant part of their bond capacity, although textile slippage within the mortar matrix occurs and the tensile capacity of the fibers cannot be fully exploited, even if the meshes are properly anchored. At 400 °C the bond capacity may be completely lost, and debonding at the matrix-to-substrate interface may occur at very low stresses, depending on the properties of each TRM.

1. Introduction

Textile Reinforced Mortars (TRM) are a relatively new generation of composites that have gained considerable attention from the scientific community in the last two decades. The system basically consists of the introduction of one or more fiber meshes embedded in a mortar matrix, resulting in a material of very little thickness (usually around 10 or 15 mm) that can be successfully used both for the strengthening of concrete [1] or masonry [2] structures. TRMs are usually composed of bi-directional meshes of glass, carbon, basalt or steel fibers (among other materials) and cementitious or lime-based mortars, sometimes enriched with polymers or short fibers. For masonry structures in particular, and compared to other strengthening solutions such as Fiber Reinforced Polymers (FRP), TRMs provide some interesting advantages: better compatibility with the retrofitted substrates, easier implementation on uneven or wet surfaces, vapor permeability, reasonable reversibility and better performance at high temperatures, for example. The effectiveness of TRMs has been successfully tested in different scenarios, such as retrofitting of walls [3–5], column confinement [6–8] and strengthening of arches or vaults [9–11], among other applications.

One of the key parameters determining the effectiveness of TRM is their bond capacity with respect to the element to be strengthened. To determine this property, composite-to-substrate bond tests are often performed with different configurations, usually single-lap or double-lap (with single or double substrate prisms) setups [12]. Among them, the single-lap setup is arguably the least complex to test and requires monitoring of just one bonded area [13], hence its implementation in the methodology adopted in the present study. In recent years, some interesting Round Robin Tests have been developed to evaluate the bond strength of TRMs with carbon [14], basalt [15], glass [16,17] or steel [17] fibers. Regarding the supporting substrate, most of the published research focused on masonry prisms built with standard clay bricks, and only two references have been found studying tuff blocks [18] or historical bricks from a century-old building [19]. Another critical issue that affects the effectiveness of TRM is the anchorage length of the meshes, an aspect that has been analyzed by means of tests with varying bond lengths [20–26]. Regarding textile density, usually a single mesh is applied, although the behavior with two or more meshes has also been reported [21,25,27,28]. Other works have focused on durability or response to adverse conditions by testing under cyclic loading [29], freeze–thaw conditions [30] or salt erosion environment [31]. Moreover, some researchers have explored the potential of innovative measurement techniques to characterize the behavior of the material, such as digital image correlation, acoustic emission or optical sensors [32–34]. As general overview of the research carried out, it is worth mentioning that the bond strength of TRM to masonry substrates is a complex issue, depending on a number of factors. Failure modes are expected to be highly variable, as established by standards and design guidelines [13,35,36], although in most cases it is initiated by textile slippage within the mortar matrix or debonding at the textile-to-matrix interface.

In the context of high temperature behavior, the non-combustible

* Corresponding author.
E-mail address: luis.estevan@ua.es (L. Estevan).

https://doi.org/10.1016/j.conbuildmat.2023.132123
Received 10 February 2023; Received in revised form 8 June 2023; Accepted 9 June 2023
Available online 13 June 2023

nature of the inorganic matrices of TRM is a clear advantage over the organic resins used with FRP [37]. Unfortunately, this feature often leads to the erroneous perception of these materials as fire-resistant solutions, when in fact this is not the case [38]. In this sense, it is worth mentioning some interesting investigations evaluating the loss of tensile strength in TRM coupons with different textile materials and matrices, after exposure to high temperatures [39–41]. Nonetheless, the information available on the bond capacity at high temperature, or after exposure to elevated temperatures, is very limited at the present time. Some authors have analyzed the bond of TRM-to-concrete substrates [42,43], although from the point of view of the objectives of this research, the works published on masonry substrates are particularly relevant: Maroudas and Papanicolaou [44], Donnini et al. [45], Ombres et al. [46], Iorfida et al. [47], Askouni et al. [48,49] and Ferretti et al. [50]. The temperature ranges in these studies are relatively moderate (up to 300 °C) and data on exposure to higher temperatures are only available in [47,49], up to 500 °C and 400 °C, respectively. These results are discussed in more detail in Section 3.3, where the characteristics of the different experimental methodologies and the main results obtained can be consulted. Consequently, it is not considered appropriate to extend this introduction unnecessarily with this information. Finally, a recent work published by some of the authors of this research [51] evaluated the behavior of masonry panels strengthened with different TRM and subjected to 600 °C. It was found that exposure to high temperatures considerably compromised the bonding of the composite material to the masonry substrate, depending on the characteristics of the meshes and the matrices involved.

Once the state-of-the-art on the bond capacity of TRM on masonry substrates after exposure to high temperatures has been analyzed, a significant knowledge gap on this subject has been identified. At the present time, this topic has hardly been investigated and very limited research has been published to date. Therefore, it is considered very appropriate to provide experimental data that will help to enrich the state of knowledge on this specific issue. For this purpose, TRMs with carbon or glass fiber textiles and different hydraulic lime mortar matrices are used on fired clay bricks substrates. Two different bond lengths are proposed, in order to analyze the behavior of sufficiently or insufficiently anchored meshes. With respect to temperature, three different exposure levels are proposed: 20, 200 and 400 °C. Finally, the experimental results are compared with those reported by the few similar investigations available at present, annotated in the previous state-of-the art introduction.

2. Materials and methods

The research presented here was carried out at the LARGE Structures Laboratory of the Civil Engineering Department of the University of Alicante (Spain). This section defines the properties of the materials used, details the planning of the experimental setup and describes the tests that were carried out.

2.1. Characterization of materials

To simulate the masonry substrate, solid fired clay bricks of dimensions 230 × 110 × 50 mm^3 were used, with a density of 1550 kg/m^3 and a compressive strength of 15 MPa, as specified by the manufacturer. The mortar used for the joints was natural hydraulic lime mortar with pozzolan, with a density of 2000 kg/m^3 and a minimum compressive strength of 7.5 MPa, according to data provided by the supplier. A total of eighteen masonry prisms were built with both materials, consisting of five brick units and four 10 mm thick mortar joints, with total dimensions of 230 × 110 × 290 mm^3.

The mechanical properties of the materials were also determined experimentally. For this purpose, six 110 × 110 × 50 mm^3 brick specimens were prepared and tested in compression according to UNE-EN 772-1:2011 + A1:2016 [52]. In addition, six 230 × 50 × 50 mm^3 specimens were tested in bending according to UNE-EN 772-6:2002 [53] and UNE-EN 1015-11:2020 [54]. For the mortar, three specimens of 160 × 40 × 40 mm^3 were manufactured and tested in bending, subsequently determining the compressive strength in the resulting six halves [54]. Finally, the compressive strength of the masonry prisms was determined by testing three specimens following the instructions of the UNE-EN 1052-1 standard [55].

All of these tests were carried out at 3 different temperature levels: 20, 200 and 400 °C, using a programmable electric furnace whose heating curves are detailed in the following section. Exceptionally, the bricks were only tested at 20 °C, because a previous investigation with the same materials [51] had shown that their strength loss after exposure to 600 °C was negligible. The results obtained are summarized in Table 1, where the corresponding coefficients of variation are included in parentheses. Note that the materials used retain their mechanical properties practically intact up to 200 °C, with a loss of strength at 400 °C of about 15% in compression and 40% in bending, with respect to unheated samples.

The TRM tested in this study included two different commercial solutions, both of which were supplied by Mapei. On the one hand, a high-strength carbon fiber mesh (Mapegrid C170, hereinafter referred to as “C”) with a two-component fiber-reinforced mortar composed by hydraulic lime, Eco-Pozzolan, natural sand, special additives and synthetic polymers in water dispersion (Planitop HDM Restauro, hereinafter referred to as “MC”). On the other hand, a pre-impregnated alkali-resistant glass fiber mesh (Mapenet EM40, hereinafter referred to as “G”) with a ready-mixed mortar made from natural hydraulic lime, reactive inorganic compounds, natural sand, special admixtures and micro-fibers (MapeWall Render & Strengthen, hereinafter referred to as “MG”). Fig. 1 shows a detail of the two meshes used and Table 2 specifies the physical and mechanical properties of the different products, according to the technical documentation provided by the manufacturer.

The mechanical properties of the meshes and mortars were determined experimentally for the three temperature levels indicated above (20, 200 and 400 °C). The bare textile meshes were tested in uniaxial tension, preparing nine samples of each type divided into three groups of three specimens for each temperature level. The samples were composed of 8 (mesh C) or 3 (mesh G) yarns, with a length of 450 mm, and were tested in warp direction in all cases. The tests were carried out in an electric press equipped with a 20 kN load cell at a constant speed of 0.3 mm per minute, recording the elongations by means of two LVDTs placed on both sides of the specimen and determining the mean value. To improve the grip of the meshes, both ends were reinforced with FRP, placing 2 layers of quadriaxial fiberglass fabric embedded in epoxy resin. The length of these reinforcements was 120 mm, leaving a central bare mesh section of 210 mm.

The resulting specimens were bolted between two 10 mm thick steel plates and the anchoring device to the press was designed to allow

Table 1
Mechanical properties of clay bricks, bed-joint mortar and masonry prisms (coefficients of variation in parentheses).

	Compressive strength (MPa)			Flexural strength (MPa)		
	at 20 °C	at 200 °C	at 400 °C	at 20 °C	at 200 °C	at 400 °C
Clay bricks	13.9 (10.4 %)	–	–	4.2 (16.9 %)	–	–
Bed-joint mortar	8.4 (8.7 %)	9.2 (6.8 %)	7.1 (10.0 %)	1.2 (14.3 %)	1.1 (7.6 %)	0.7 (16.9 %)
Masonry prisms	8.8 (4.8 %)	8.5 (9.5 %)	7.9 (5.3 %)	–	–	–

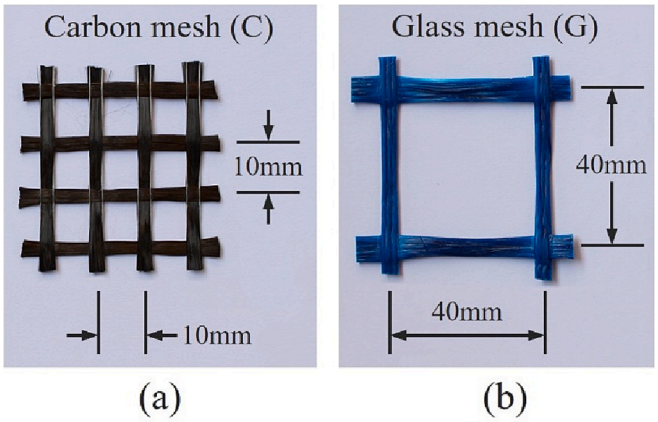

Fig. 1. Detail of the textiles used: (a) high-strength carbon fiber mesh; (b) A.R. glass fiber mesh.

Table 2
Properties of TRM textiles and mortars (values provided by the manufacturer).

	Textile		Matrix mortar	
	C	G	MC	MG
Type of fiber	high-strength carbon fiber	alkali-resistant glass fiber	–	–
Mesh size (mm)	10 × 10	40 × 40	–	–
Weight (g/m^2)	170	270	–	–
Load-resistant area (mm^2/m)	48	35.82		
Area of single yarn (mm^2)	0.48	1.52	–	–
Tensile strength (kN/m)	> 240	56.25	–	–
Tensile strength (MPa) [a]	> 5000	1570	–	–
Elongation at failure (%)	2	4	–	–
Modulus of elasticity (GPa)	252 ± 2%	33	8	10
Compressive strength (MPa)	–	–	> 15	> 15
Bond strength to substrate (MPa)	–	–	≥ 0.8	≥ 1

[a] Values not supplied, obtained from tensile strength (kN/m) and load-resistant area (mm^2/m).

rotation at both ends, in order to correct possible eccentricities or centering errors. The stress–strain curves obtained for the carbon (Fig. 2a) and glass (Fig. 2b) fiber meshes under the three temperature levels considered are shown in Fig. 2. The experimental results are summarized in Table 3, including the corresponding coefficients of variation in parentheses. As can be seen, the carbon fiber meshes maintain their properties intact up to 200 °C and only show a slight strength loss (less than 15%) at 400 °C, with the modulus of elasticity almost intact. However, the behavior of the glass fiber meshes is clearly

Table 3
Experimental results for bare textiles exposed to 20, 200 and 400 °C (coefficients of variation in parentheses).

ID	C20	C200	C400	G20	G200	G400
Exposure temperature	20 °C	200 °C	400 °C	20 °C	200 °C	400 °C
Tensile strength (MPa)	2894 (0.6 %)	2927 (4.1 %)	2501 (4.0 %)	1397 (4.3 %)	1401 (1.4 %)	374 (2.1 %)
Elongation at failure (%)	1.07 (3.4 %)	1.02 (3.6 %)	0.83 (1.9 %)	1.73 (5.5 %)	1.43 (0.9 %)	0.39 (7.0 %)
Modulus of elasticity (GPa)	289 (2.5 %)	304 (3.4 %)	328 (0.4 %)	97 (1.5 %)	102 (1.3 %)	95 (2.5 %)

Table 4
Experimental results for TRM mortars exposed to 20, 200 and 400 °C (coefficients of variation in parentheses).

ID	MC			MG		
Exposure temperature	20 °C	200 °C	400 °C	20 °C	200 °C	400 °C
Compressive strength (MPa)	16.9 (5.4 %)	15.7 (20.7 %)	7.1 (12.1 %)	9.6 (15.9 %)	8.4 (16.3 %)	8.8 (17.1 %)
Flexural strength (MPa)	5.3 (13.3 %)	5.5 (11.9 %)	2.4 (9.9 %)	4.0 (10.7 %)	3.1 (4.1 %)	2.9 (6.8 %)
Modulus of elasticity (GPa)[a]	8.6 (4.5 %)	6.9 (3.5 %)	3.8 (4.4 %)	10.3 (2.2 %)	8.3 (1.9 %)	6.5 (1.9 %)

[a] Dynamic modulus from ultrasonic tests in 160x40x40 mm^3 mortar samples.

different, showing a strong degradation of the material at 400 °C, with strength losses of more than 70%. It should be noted that the tensile strength of the carbon fiber mesh tested at room temperature is significantly lower than the value provided by the manufacturer (Table 1); this is not the case with the glass fiber mesh, in which only a difference of about 12% was obtained.

The mortars used in the TRM systems were also tested experimentally. The results were reported in a previous research published by the authors of the present work [41] and are summarized in Table 4. To determine the mechanical properties, series of three prismatic specimens of 160 × 40 × 40 mm^3 were prepared for each type of mortar and temperature level, which were subsequently tested in bending and compression by the same procedure indicated above [54]. Prior to the mechanical tests, the dynamic modulus of elasticity was determined by ultrasonic wave propagation tests on the same specimens, according to ASTM D2845-08 [56]. The test procedure, an image of the equipment used, and the formulation used for the calculation of the dynamic modulus of elasticity can be found in [41]. The results show that the MC mortar performed well up to 200 °C, although it underwent a strong degradation at 400 °C, with a decrease of almost 60% in both strength and modulus of elasticity. In turn, the MG mortar appeared to withstand the effect of temperature better, both in terms of strength and stiffness. As discussed in [41], the liquid phase of the MC mortar is composed of synthetic polymers in water dispersion, which exhibit a significant

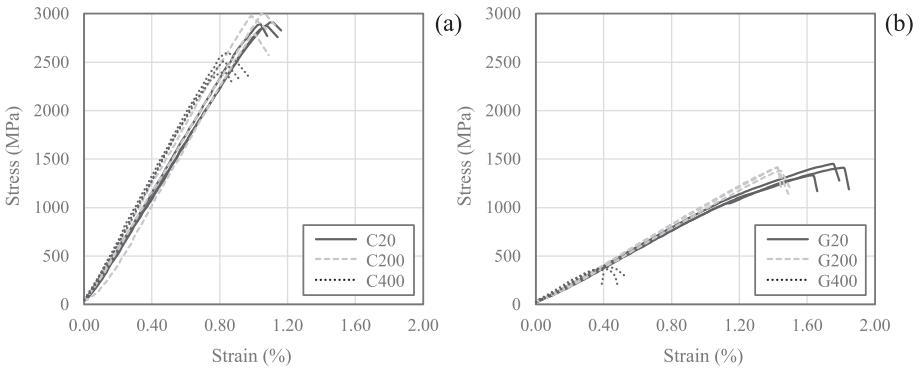

Fig. 2. Stress–strain curves obtained experimentally for bare textiles exposed to 20, 200 and 400 °C: (a) carbon fiber mesh; (b) glass fiber mesh.

degradation at temperatures above 200 °C; on the other hand, this mortar is reinforced with polypropylene fibers, which are highly affected by heat and largely determine the flexural strength of the material. For these reasons, MC mortar is more sensitive to exposure to high temperatures than MG.

2.2. Experimental program and exposure to high temperature

For the experimental program of this research, eighteen masonry prisms composed of five brick units of total dimensions 230 × 110 × 290 mm^3 were prepared, as explained in the previous section. All specimens were kept for a 90-day period in ambient laboratory conditions, in order to allow sufficient curing of the natural hydraulic lime mortar used for the joints. After that, the surface of the panels was prepared by removing loose mortar residue, dust and dirt using a steel wire brush and compressed air. The installation of the TRM is illustrated in Fig. 3a, which shows the application of one of the glass fiber meshes, adopting the recommendations of RILEM TC 250-CSM [13]. First, the surface of the masonry was saturated with water to prevent moisture loss from the mortar mass by absorption. Next, a first layer of mortar about 5 mm thick was applied inside a mold to precisely define the desired bond width and length. With the mortar still fresh, the reinforcing mesh was placed, applying light pressure and making sure that the yarns were perfectly aligned and centered in the specimen. A second 5 mm layer of mortar was then applied and smoothed with a smooth-edged metal trowel, resulting in a total thickness of the TRM of approximately 10 mm. A scheme with the geometry and dimensions of the specimens is shown in Fig. 3b. It can be observed how in all cases a free length of 400 mm of unbonded textile was maintained, as well as a distance of 30 mm between the beginning of the bonded area and the edge of the masonry prism [13]. The free end of the meshes in the gripping area was left embedded between two layers of FRP, made of quadriaxial glass fiber fabric and epoxy resin, with a length of 120 mm. The width of the bonded area (B) was 100 mm in all cases, a dimension that allowed accommodating eight yarns (carbon fiber mesh, with a narrower pitch) or three yarns (glass fiber mesh, with a wider pitch). As shown in Fig. 3b, a TRM was applied on each of the main faces of the wall, with two different bonding lengths ($L_1 = 250$ mm and $L_2 = 150$ mm), to simulate the case of sufficiently or insufficiently anchored meshes on the substrate. To define these lengths, the ACI 549.6R-20 [36] guidelines were followed, which establishes an effective bond length in the range of 200 to 250 mm; on the other hand, the recommendations of RILEM TC 250-CSM [13] were also considered, where it is indicated that bond lengths shorter than 250 mm may be insufficient and are therefore not recommended. It should be noted that the lengths defined in both documents are generic and independent of the type of mesh used. In all cases a single layer of reinforcement was placed and, of the two textiles used, only mesh C was pre-impregnated with the liquid phase of the MC mortar, in order to increase adherence and following the manufacturer's recommendations (mesh G is coated and does not require such pre-impregnation). Finally, once the installation of the TRM was completed, the exposed mortar surfaces were protected with polyethylene sheets to preserve humidity and were kept for 7 days. Furthermore, the specimens were kept in ambient laboratory conditions for a total of 60 days before starting the bond tests, which are detailed in the following section.

The experimental campaign was designed on the basis of twelve series and three specimens per series, with the codification given in Table 5. The first letter indicates the type of mesh used (C or G). Next, the exposure temperature level is defined (20, 200 or 400 °C). Next, the bond length adopted is specified (150 or 250 mm). Finally, the number of the specimen within each series is indicated (1, 2 or 3). For example, reference C200-150-3 denotes a TRM with carbon fiber mesh exposed at 200 °C, with a bond length on the substrate of 150 mm, and specimen number 3.

For the definition of the indicated temperature levels, the results reported in [41] were considered, where coupons produced with the same materials were studied in tensile tests after exposure to 100, 200, 400 and 600 °C. In this research it was found that both TRMs retained their properties relatively unaltered at 200 °C, were significantly affected by exposure to 400 °C, and lost all their mechanical capacity at 600 °C as a consequence of the total degradation of the meshes. For this reason, the maximum exposure temperature in the present work was limited to 400 °C. All the series subjected to high temperatures were previously treated with thermal insulation to preserve the integrity of the meshes and prevent distortions in the bond tests to be carried out later. Fig. 4a shows the solution adopted, which basically consisted of placing mineral wool and temperature-resistant aluminum foil tape, keeping the bonded area of the TRM exposed to the brick substrate. However, in order to avoid deterioration of the unbonded textile, a 20 mm overlap was provided as shown in the sketch. Fig. 4b shows an image of the specimens inside the furnace, which were arranged in pairs. For temperature monitoring, one specimen of each series was instrumented with three thermocouples connected to a computer-controlled data acquisition unit. Thermocouple A was placed adhered to the mortar matrix of the TRM, thus measuring the air temperature inside the furnace. Additionally, thermocouples B and C were installed next to the unbonded textile inside the thermal insulation, in order to register the maximum temperature reached by the meshes. The furnace was programmed at an increasing heating rate of 10 °C per minute until the target temperature was reached, remaining constant for 1 h. The heating rate and exposure time of samples was the same as that considered in

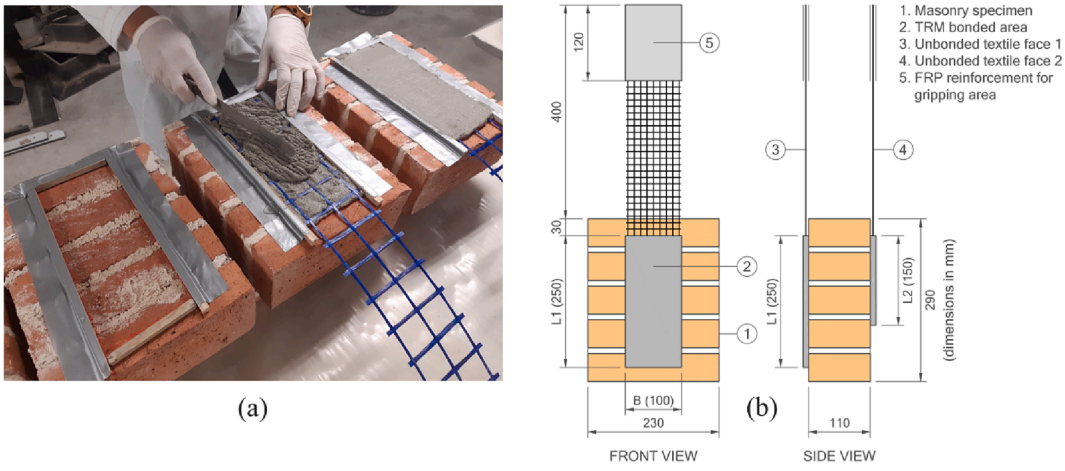

Fig. 3. Production of specimens: (a) TRM installation process on the masonry substrate; (b) geometry and dimensions scheme.

Table 5
Summary of experimental campaign and nomenclature of specimens.

ID	Textile	Matrix mortar	Temperature (°C)	*B* (mm)	*L* (mm)	Samples
C20-150	C	MC	20	100	150	3
C20-250					250	3
C200-150	C	MC	200	100	150	3
C200-250					250	3
C400-150	C	MC	400	100	150	3
C400-250					250	3
G20-150	G	MG	20	100	150	3
G20-250					250	3
G200-150	G	MG	200	100	150	3
G200-250					250	3
G400-150	G	MG	400	100	150	3
G400-250					250	3
Total samples						36

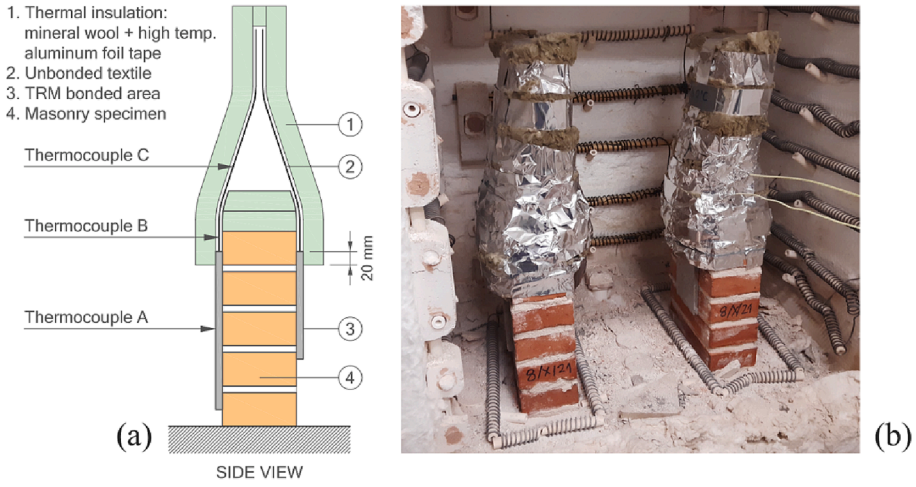

Fig. 4. Exposure of samples to high temperature: (a) thermal insulation scheme and thermocouples arrangement; (b) image of the specimens inside the furnace.

[41], and very similar to that defined in other similar works [49]. Once the programmed heating cycle was completed, the furnace was switched off and the specimens were kept inside for 24 h until reaching the ambient temperature of the laboratory; consequently, the bond tests were carried out with the samples at room temperature in all cases. Fig. 5 shows the temperature curves recorded by the three thermocouples in the different series studied. As can be seen, in the specimens exposed to 400 °C the meshes did not reach the temperature of 200 °C at any time. In turn, in the specimens exposed to 200 °C, the fabrics underwent maximum temperatures of 100 °C, approximately. In view of the results obtained, and taking into account the behavior of the bare textiles at these temperature levels (Fig. 2 and Table 3), it might be concluded that the meshes were sufficiently protected with the thermal insulation solution adopted.

Finally, as mentioned in the precedent paragraph, the bond tests in this research were performed 24 h after exposure to high temperatures, i.e., the samples were tested at room temperature. In this regard, it would be worthwhile to analyze the TRM-to-masonry bond on the samples tested at the target temperature. To the authors' knowledge, this effect has hardly been explored so far and only two studies have reported data on this topic [45,50]. However, the maximum temperature reached in these studies was 120 and 80 °C, respectively, which is far from the exposure levels used in the present work. Obviously, to perform these tests, a thermo-mechanical machine (i.e., a press equipped with a furnace which can simultaneously generate the mechanical and thermal loadings) is required. Further research on this issue will be

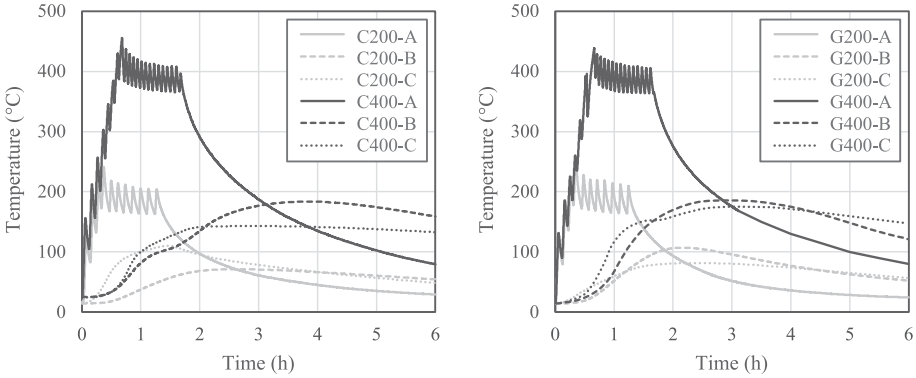

Fig. 5. Temperature curves recorded on the exposed surface of TRMs (thermocouple A) and on textiles inside the thermal insulation (thermocouples B and C).

of interest in the future.

2.3. Test setup and instrumentation

To characterize the TRM-to-substrate bond behavior a single-lap shear setup was designed, in accordance with RILEM TC 250-CSM [13]. Fig. 6 shows an image and a front and side scheme of the test setup. The masonry prism was inserted between two 15 mm thick steel plates and was secured in place by four 12 mm diameter threaded rods. The free end of the unbonded textile, provided with FRP reinforcement as explained above, was anchored between two 10 mm thick steel plates with six screws of 10 mm diameter. These plates were connected to the test rig by means of a pin to release the rotation, thus compensating for slight eccentricities or centering errors of the specimens. The tests were carried out on an electric press equipped with a 20 kN capacity load cell, programmed under displacement control at a constant speed of 0.3 mm per minute. Prior to each test, a preload of 0.25 kN was applied to slightly put the mesh in tension and to verify its proper alignment with the vertical axis of the press.

Two LVDTs bolted to an 8 mm thick steel plate were used to record the deformations, as shown in Fig. 6. These LVDTs reacted against an aluminum L-shaped profile (each side of the L was 30 mm long and 2 mm thick), that had been attached to the mesh using an epoxy resin 24 h prior to each test. The deformations were recorded using an HBK QuantumX MX1615B data acquisition system, programmed at a sampling rate of 2 Hz.

3. Results and discussion

This section presents and discusses the experimental results, analyzing the failure modes obtained and the bond behavior as a function of the exposure temperature. The discussion is completed with a comparative study with the few similar investigations published to date.

3.1. Failure modes

The classification proposed by the Italian guide CNR-DT 215/2018 [35] is followed for the identification of the failure modes obtained. These failures depend both on the properties of the supporting substrate and on the characteristics of the TRM used, and usually match the modes represented in Fig. 7. Basically, the failure may occur by debonding: (A) with cohesive failure of the substrate; (B) at the matrix-to-substrate interface; or (C) at the textile-to-matrix interface. Textile slippage with respect to the matrix may also occur: (D) without mortar cracking; or (E) with cracking of the outer layer of mortar. Finally, another frequent failure mode is due to tensile rupture of the textile, usually out of the bonded area (F). A more detailed discussion of the different failure modes listed can be found, for example, in reference [12].

Fig. 8 shows an example of the failure modes obtained in the 12 series tested. It is important to note that only the tensile rupture of the fabric (failure mode F) occurred in the C20-250 (Fig. 8b) and G20-250 (Fig. 8d) series, whereas in the rest of the cases the meshes were cut manually after each test to facilitate the visualization of the specimens. By first analyzing the response of the TRM at room temperature, it was observed that the failure mode depended directly on the adopted bond length (L), both with carbon fiber and glass fiber meshes. When length L was sufficient, tensile failure of the mesh would occur, as mentioned above, while the mortar matrix remained intact in all cases (Fig. 8b and d). In case of insufficiently anchored meshes, either the mesh slipped away from the matrix, which remained intact (failure mode D, Fig. 8a) or the outer mortar layer broke (failure mode E, Fig. 8c), depending on the TRM used. It may therefore be concluded that it is very important to provide the meshes with a sufficient anchorage length, if the mechanical capacity of the fibers is to be fully exploited. In this sense, the bond length proposed in this work (L = 250 mm) was consistent with the recommendations of ACI 549.6R-20 [36], which establishes a length of 200 to 250 mm, or RILEM TC 250-CSM [13], where it is indicated that bond lengths shorter than 250 mm may be insufficient and are therefore not recommended.

After exposure to 200 °C, it was found that failure occurred either by slippage of the meshes in all the series, with the matrix intact in case of the carbon fiber fabrics (failure mode D, Fig. 8e and f) or with cracking of the outer layer of mortar in case of the glass fabrics (failure mode E, Fig. 8g and h). The fundamental difference with respect to the series tested at 20 °C lies in the fact that the fibers were not able to fully develop their tensile strength even if they were properly anchored, since the bond between the fabric and the mortar would appear to be compromised at this temperature level. As for TRM with L = 150 mm, it

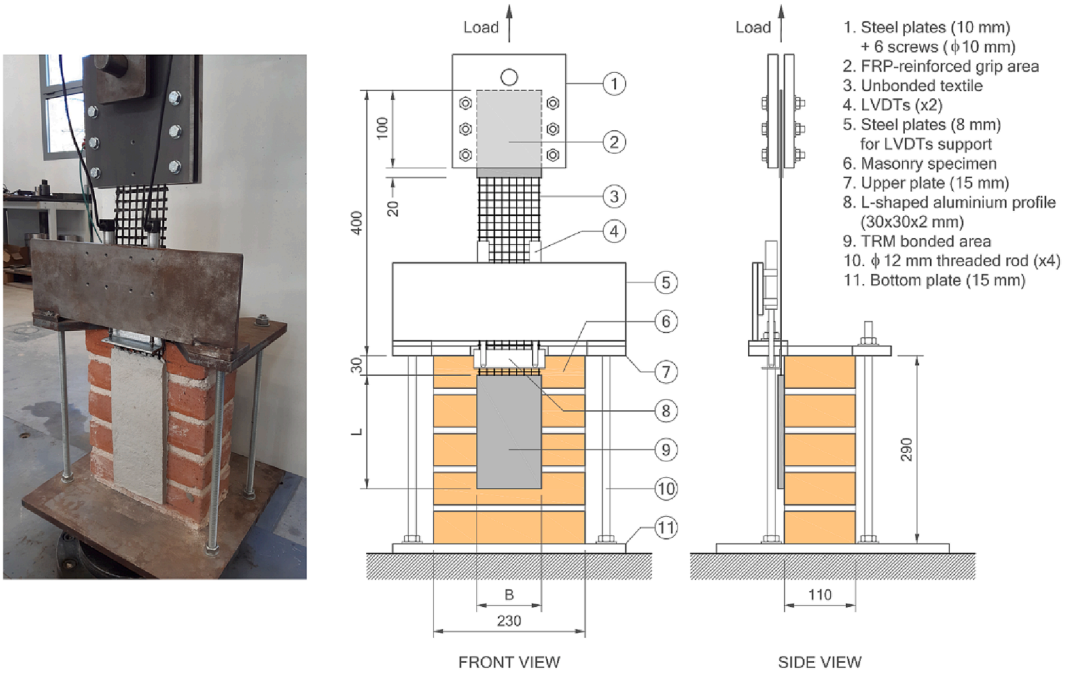

Fig. 6. Image and front and side scheme of test setup.

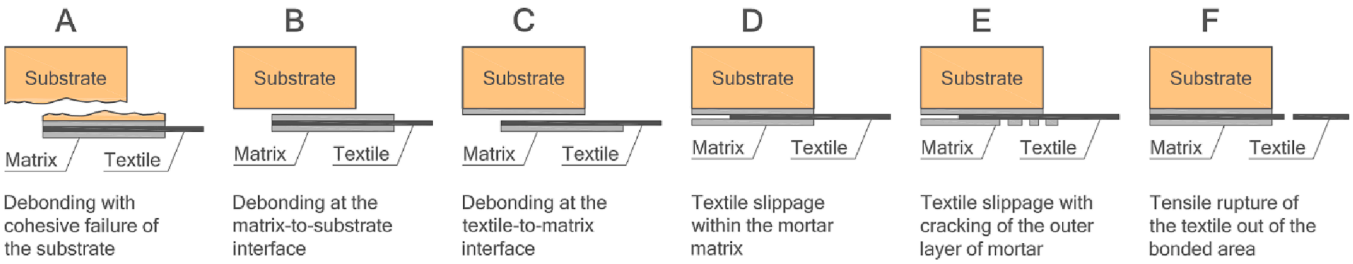

Fig. 7. Failure modes according to Italian guide CNR-DT 215/2018.

Fig. 8. Failure modes obtained in all series (meshes were cut manually after testing, except in case of textile tensile failures).

can be seen that the failure modes were exactly the same as those exhibited by the series tested at 20 °C, although greater deterioration of the outer mortar layer was observed in the G200-150 series (Fig. 8g).

Finally, in the series exposed to 400 °C, a drastic change in the failure mode of the carbon fiber TRM was observed, producing the debonding of the mortar matrix from the brick substrate at very low load levels, and independently of the bond length adopted (failure mode B, Fig. 8i and j). These results are consistent with the conclusions of a previous investigation with the same materials [41], where it was found that the MC mortar suffers a strong loss of mechanical properties at 400 °C and above, basically due to the presence of synthetic fibers and polymers in its composition. It can be concluded, therefore, that TRM completely loses all its bonding capacity at these temperature levels. In turn, it was observed that the failure modes of the glass fiber TRM were similar to

those obtained at 200 °C, although the outer layer of the mortar matrix tended to exhibit greater deterioration. Moreover, a darkening and a certain degradation of the polymer coating of the mesh was perceived (Fig. 8k and l). In this regard, it should be mentioned that the MG mortar preserved its mechanical properties relatively intact at 400 °C [41].

3.2. Stress-slip relationship and bond capacity

The results of the bond tests are shown in Fig. 9 corresponding to all the specimens studied. In these graphs the axial stress (on the y-axis) was obtained as the applied load divided by the cross-section area of the load-aligned fibers of the textile (Table 2), i.e., 3.84 mm^2 (8 yarns in mesh C) and 4.56 mm^2 (3 yarns in mesh G). With respect to slip (on the x-axis), it was calculated as the average of the displacements measured by the two LVDTs [13]. The experimental results are summarized in Table 6 as follows: peak load (F_b) and peak axial stress (f_b); textile tensile strength (f_t); exploitation ratio ($\eta = f_b / f_t$); mean ultimate shear stress at the composite-to-substrate interface (τ_{bm}), calculated as the peak load divided by the bonded area ($B \times L$); peak slip (s_b), i.e., slip corresponding to the peak axial stress; and failure mode obtained in each series, as described in previous section. Regarding the definition of the exploitation ratio, there is no clear consensus among the different published investigations: some authors obtain it with respect to the tensile strength of the fibers [14,21,23,26–28,49], others with respect to the axial stress derived from tensile tests on TRM coupons [12,16,17,29,44], or even using both approaches [15,19,32]. In this work, the tensile strength of the fabric (f_t) is adopted for each temperature level considered (Table 3), which is presented as a dashed line in the graphs of Fig. 9, to facilitate the visualization of the exploitation ratios obtained.

At room temperature (Fig. 9a and b), it was observed that TRM with sufficient bond length exhibited an approximately linear response and sudden breakage (failure mode F) at stress close to the tensile strength of the fabric, with $\eta = 0.84$ (C) and $\eta = 0.88$ (G). Hence, it would mean that the mechanical capacity of the meshes might be almost fully exploited under these conditions. The linear behavior was much more evident with the glass fiber meshes, while the carbon fiber meshes suffered the rupture of some fibers during the course of the test at stresses above 2000 MPa, which resulted in a more or less pronounced staggering in the stress-slip curves. As for the meshes with $L = 150$ mm, it was observed that the curves displayed a very different response, due to the slip of the fibers with respect to the mortar matrix (failure modes D-E). Furthermore, this case revealed a post-peak phase characterized by a somewhat steeper downward curve with the carbon fiber specimens. The exploitation ratios seem to indicate that the meshes work at approximately half their mechanical capacity, namely $\eta = 0.46$ (C) and $\eta = 0.50$ (G). Thus, it is appropriate to insist again on the idea of providing a sufficient

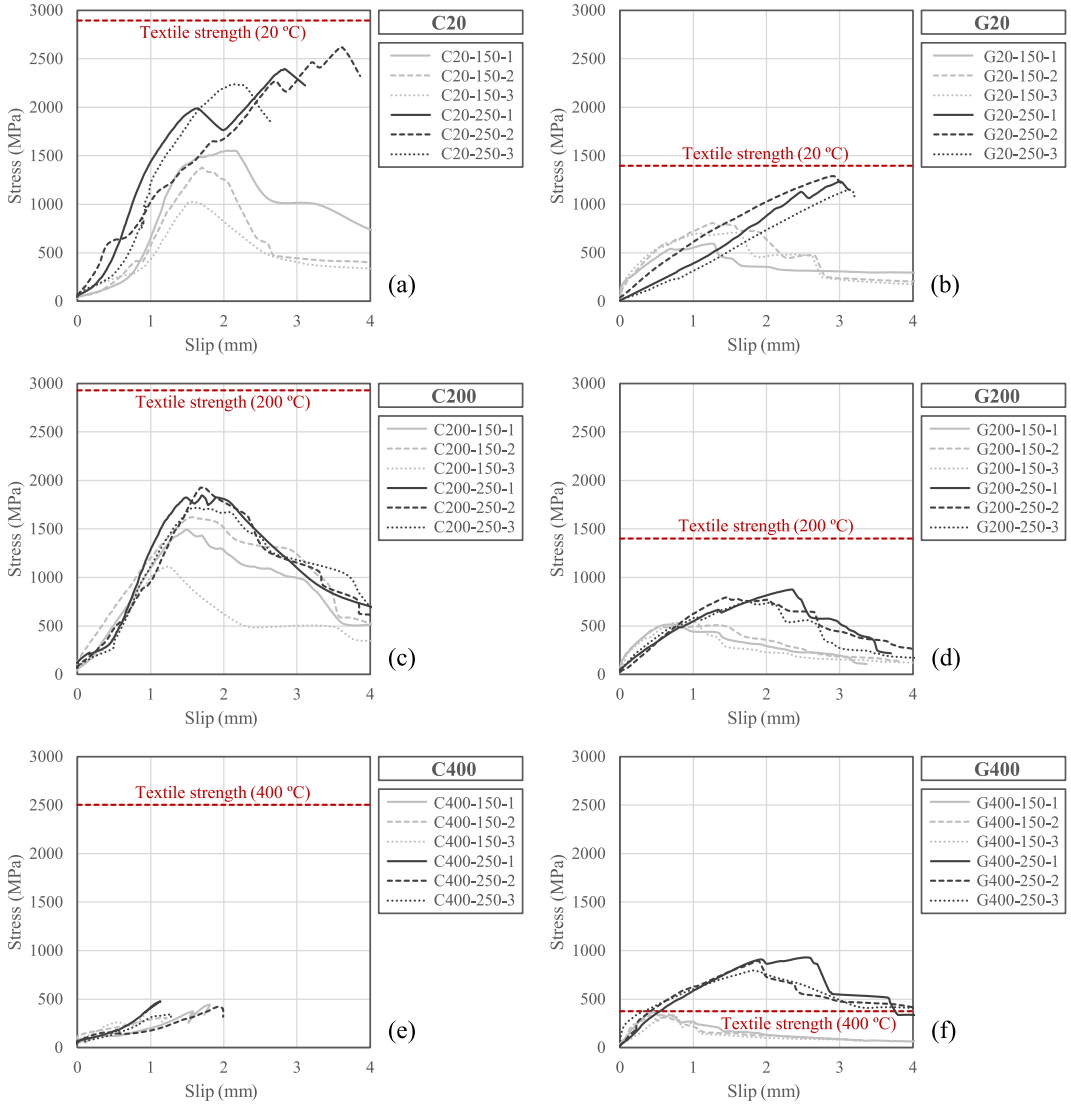

Fig. 9. Stress-slip curves for all samples tested.

Table 6
Experimental results from bond tests (coefficients of variation in parentheses).

ID	F_b (kN)	f_b (MPa)	f_t (MPa)	$\eta = f_b / f_t$	τ_{bm} (MPa)	s_b (mm)	Failure mode
C20-150	5.06 (20.3 %)	1319	2894	0.46	0.34	1.81 (17.0 %)	D
C20-250	9.29 (7.9 %)	2419		0.84	0.37	2.86 (25.4 %)	F
C200-150	5.41 (18.7 %)	1408	2927	0.48	0.36	1.43 (11.9 %)	D
C200-250	7.03 (5.7 %)	1831		0.63	0.28	1.69 (2.7%)	D
C400-150	1.54 (20.0 %)	401	2501	0.16	0.10	1.34 (30.3 %)	B
C400-250	1.59 (16.5 %)	413		0.17	0.06	1.43 (30.2 %)	B
G20-150	3.20 (15.2 %)	704	1397	0.50	0.21	1.36 (13.4 %)	E
G20-250	5.58 (5.8 %)	1225		0.88	0.22	3.01 (3.5 %)	F
G200-150	2.38 (3.6 %)	522	1401	0.37	0.16	1.00 (29.9 %)	E
G200-250	3.68 (7.9 %)	808		0.58	0.15	1.86 (24.0 %)	E
G400-150	1.58 (5.6 %)	348	374	0.93	0.11	0.51 (25.9 %)	E
G400-250	3.97 (8.0 %)	872		2.33	0.16	2.08 (18.6 %)	E

anchorage length of the meshes to optimize the bond capacity of the TRM on the brick substrate.

After exposure to 200 °C (Fig. 9c and d), it was found that the carbon fiber meshes exhibited approximately the same behavior, regardless of the bond length adopted. The curves indicated a linear response up to the peak stress, beyond which a post-peak phase similar to that observed in the C20-150 series, as a consequence of the textile slippage with respect to the mortar matrix (failure mode D). The exploitation ratios, between 0.48 and 0.63, denote a significant loss of bond at this temperature level, even if the meshes had been correctly anchored. With respect to the glass fiber fabrics, the bond length seemed to have a greater impact, with coefficients $\eta = 0.37$ (G200-150) and $\eta = 0.58$ (G200-250). The curves again showed a descending branch after the peak stress, due to fiber slippage with progressive cracking of the outer layer of the mortar matrix described in the previous section (failure mode E). Thus, it may be inferred that although the tensile strength of the bare textiles at 20 or 200 °C did not show any difference (Table 3, Fig. 2 and Fig. 9), this temperature level did compromise the bond capacity between the fibers and the mortar matrix, significantly reducing the effectiveness of the TRMs studied.

As regards the series subjected to 400 °C (Fig. 9e and f), the large difference observed between the carbon and glass fiber meshes was striking. In the first case, the curves reflected the debonding of the mortar matrix from the brick substrate at very low stresses (failure mode B). It would seem evident that the result is independent of the anchorage length adopted. It can be concluded, as previously mentioned, that the TRM completely lost all its bond capacity at this temperature level. Considering this, it could be interesting to study the possibility of including connectors between the TRM and the substrate, an aspect that lies outside the scope of this paper and that is proposed as a possible line of investigation for future research. With respect to the glass fiber meshes, the response was very similar to that identified in the series exposed at 200 °C, with the same failure mode E described above. Nevertheless, it should be noted that in the fully anchored meshes an abnormally high exploitation ratio ($\eta = 2.33$) was measured, when compared to the tensile strength of the bare textile subjected to 400 °C (Fig. 2 and Table 3). A possible explanation for this is that these meshes were deeply damaged when directly exposed to this temperature level, resulting in the complete degradation of the polymer coating of the fibers. However, the effect of embedding the fabric in the mortar matrix and subsequently exposing the TRM on just one side by adhering it to the brick substrate, would allow relative protection of the meshes from the heat and, therefore, less real degradation (Fig. 8k and l).

To analyze the effect of temperature on the bond behavior of the studied TRMs, Fig. 10 shows the evolution of peak stress (f_b), peak slip (s_b) and exploitation ratio (η), in terms of normalized residual values, for the three temperature levels considered in this work (20, 200 and 400 °C). In the series subjected to 200 °C, leaving aside the particular case C ($L = 150$ mm) that presented some anomaly, a good homogeneity in the results was observed. The losses range between 24% and 34% (f_b), between 26% and 41% (s_b) and between 25% and 34% (η). It may therefore be assumed that the TRMs retained a significant portion of their bond capacity at this temperature level. At 400 °C, however, the results showed greater dispersion. In terms of peak stress, the 83% decrease suffered by the C series ($L = 250$ mm), which lost practically all its bond strength, is particularly noteworthy. In contrast, the G series ($L = 250$ mm) exhibited better behavior and the loss (29%) was even lower than that obtained at 200 °C. Therefore, it seems that in this case the TRM did retain a good portion of its bond capacity at this temperature. With respect to the peak slip, a greater homogeneity was observed, with reductions between 26% and 62%. Finally, as regards the exploitation ratio η, the maximum decrease suffered by the carbon fiber meshes (80%) differs from the notable increase registered in the glass meshes, although this increase is mainly attributed to the way in which the coefficient had been estimated, as mentioned above. It should be noted that the improvement of mechanical properties of the TRM with glass fiber meshes after exposure to high temperatures had already been observed in tensile coupons tested with the same materials [41]. This improvement usually occurs with polymer-coated meshes, in which the bond between the fibers and the mortar matrix is increased when the coating is softened by the effect of heat (in the dry carbon fiber mesh used in this work this effect was not found).

Finally, to easily visualize the correlation between the failure modes obtained and the results from bond tests, the relationship between peak stress (f_b) and peak slip (s_b) for carbon (Fig. 11a) or glass (Fig. 11b) fiber meshes is plotted, identifying the failures presented in Section 3.1. Regarding the carbon fiber meshes, the maximum stress and slip peaks (2500 MPa and 3 mm, approximately) are obtained for the C20-250 series, in correspondence with the tensile rupture of the fibers (failure mode F). As for the C20-150 series and the specimens subjected to 200 °C, a clear loss of efficiency was observed, with peak stresses between 1000 and 2000 MPa, and peak slips in the range of 1 to 2 mm, the failure being due to slippage of the fibers with respect to the mortar matrix (failure mode D). At 400 °C, the TRM can be considered to have lost almost all its bonding capacity, with maximum stresses below 500 MPa and failure due to debonding at the textile-to-matrix interface (failure mode B). With respect to the glass fiber meshes, it can be seen how the maximum stress and slip peaks (1250 MPa and 3 mm, approximately) are again obtained in the G20-250 series, with tensile rupture of the fibers (failure mode F). In the rest of the series, collapse was produced by slippage of the fibers with cracking of the outer layer of the mortar matrix (failure mode E), and it was clearly observed how bond was dramatically reduced in the case of insufficiently anchored meshes.

3.3. Comparison with other studies

Finally, it is deemed appropriate to compare the experimental results presented in the previous sections with those reported in other similar investigations. As explained in the introduction, published works on the

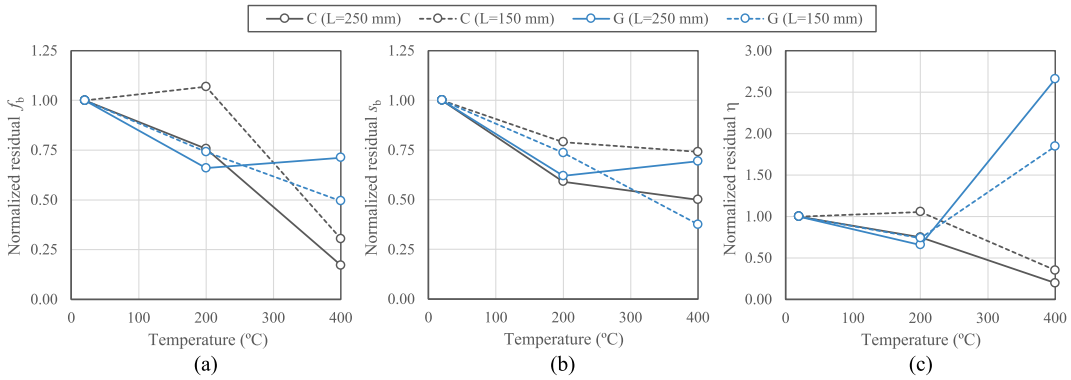

Fig. 10. Evolution of peak axial stress (f_b), peak slip (s_b) and exploitation ratio (η) with temperature increase.

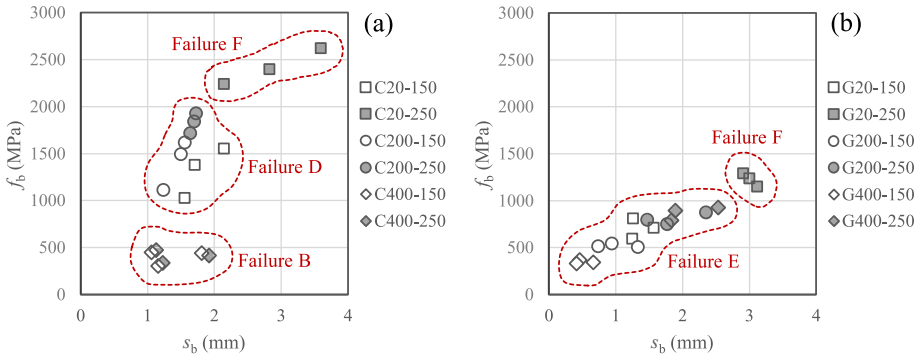

Fig. 11. Peak stress (f_b) – peak slip (s_b) relationship and identification of failure modes.

bond capacity of TRM on brick substrates after exposure to high temperatures are scarce at the present time, so the available information is limited. For comparison, the investigations of Mauroudas and Papanicolaou [44], Ombres et al. [46], Iorfida et al. [47] and Askouni et al. [49] have been selected. Two other papers in this line have been left out of the study, as the temperature ranges adopted are relatively low: Donnini et al. [45] and Ferretti et al. [50], with maximum exposure temperatures of 120 and 80 °C, respectively. Another similar research published by Askouni et al. [48] has not been considered either, as the maximum temperature level is 200 °C, compared to 400 °C in the selected reference [49]. Table 7 summarizes the main characteristics of the materials used in these works, and the values of peak stress (or peak load) as a function of the different temperatures reported. It should be noted that variable bond lengths are involved in some of the selected studies. In these cases, only the length closest to the one used in the present investigation for sufficiently anchored meshes ($L = 250$ mm) has been considered, as specified in Table 7. Masonry prisms made of clay bricks were used to simulate the substrate in all cases.

Fig. 12 shows the bond drops registered in this study, for both carbon and glass fiber meshes, together with those reported in the different works considered, as a function of the exposure temperature. The analysis has been made in terms of normalized residual peak stress (or peak load). Obviously, this comparison should be considered basically in qualitative terms and with caution. As discussed in previous sections,

Table 7
Summary of experimental campaigns in other studies.

ID	Ref.	Mortar matrix	Textile (weight)	Bond length (mm)	Peak stress (MPa) or peak load (kN) [a]						
					20 °C	100 °C	150 °C	200 °C	300 °C	400 °C	500 °C
Maroudas and Papanicolaou	[44]	Cement-based mortar, polymers and fibers	Glass (320 g/m^2)	250	3.89	2.26	–	2.38	1.48	–	–
Ombres et al. (I)	[46]	Hydraulic lime mortar and polymers	Basalt (200 g/m^2)	300	882	864	809	766	–	–	–
Ombres et al. (II)	[46]	Hydraulic lime mortar and polymers	Basalt (400 g/m^2)	300	475	333	270	251	–	–	–
Ombres et al. (III)	[46]	Cement based mortar	PBO (44 g/m^2)	300	2320	2020	1770	1520	–	–	–
Iorfida et al. (I)	[47]	Fiber-reinforced inorganic matrix	Carbon (168 g/m^2)	300	1324[b]	985[b]	–	–	844[b]	–	510[b]
Iorfida et al. (II)	[47]	Mineral NHL mortar	Basalt (200 g/m^2)	300	1020[b]	791[b]	–	–	909[b]	–	265[b]
Iorfida et al. (III)	[47]	Mineral NHL mortar	Basalt (400 g/m^2)	300	682[b]	501[b]	–	–	593[b]	–	232[b]
Askouni et al. (I)	[49]	Cement based mortar and fibers (normal weight)	Glass (300 g/m^2)	250	378	–	–	332	–	178	–
Askouni et al. (II)	[49]	Cement based mortar and fibers (light weight)	Glass (300 g/m^2)	250	391	–	–	321	–	182	–
Askouni et al. (III)	[49]	Alkali activated mortar and fibers (normal weight)	Glass (300 g/m^2)	250	531	–	–	428	–	286	–
Askouni et al. (IV)	[49]	Alkali activated mortar and fibers (light weight)	Glass (300 g/m^2)	250	561	–	–	415	–	246	–

[a] Peak stress in all cases except for Maroudas and Papanicolaou, where only peak load is provided.
[b] Approximate values measured from a figure, as no table of results is available in the paper.

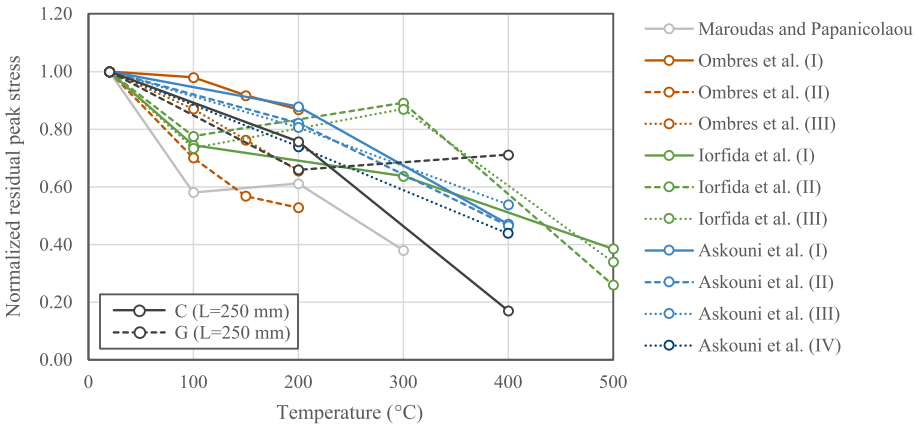

Fig. 12. Evolution of peak axial stress (f_b) with temperature increase: comparison with other studies.

aspects such as the composition of the mortars or the coating of the fabrics may significantly affect the results. A rigorous comparison would only be valid between TRMs with identical composition, and tested under the same conditions. As can be seen, the results show an acceptable homogeneity at moderate temperatures (up to 200 °C). As discussed in previous section, bond drops at this exposure level range from 24% (C) to 34% (G), and these results fall in the average of the decreases reported by the rest of the investigations. However, at higher temperatures it becomes evident that the dispersion of the results increases considerably. At 400 °C the bond drop obtained with the carbon fiber meshes (83%) is much more pronounced than those registered in other studies. This loss is undoubtedly due to debonding at the matrix-to-substrate interface (Failure B) at very low stress levels, as explained in previous sections. The TRMs with glass fiber meshes, on the other hand, seem to retain a good part of their bond capacity at this temperature and the drops obtained (29%) are lower than those presented in other works. The decreases reported by the only studies that reached these temperature levels, Iorfida et al. [47] and Askouni et al. [49], range between 40% and 56% at 400 °C, respectively.

Finally, it should be noted that the failure modes reported in the different selected works are highly variable and no clear pattern of behavior emerges. Normally, failure occurs by slippage of the fibers with respect to the mortar matrix (failure mode D) or rupture of the fibers outside the bonded zone (failure mode F), while debonding at the matrix-to-substrate (failure mode B) has only been reported in the work of Mauroudas and Papanicolaou [44]. It is important to note that, in most of the cases studied, failure modes did not depend on the level of exposure temperature. The only series in which variable failure modes have been reported with increasing temperatures are Mauroudas and Papanicolaou, Ombres et al. (III) and Iorfida et al. (III). Further research would be necessary in the future to establish predictable behavior patterns because, as mentioned above, the information available at present is very scarce on this topic.

4. Conclusions

This paper has analyzed the influence of temperature on the bonding capacity of different TRM solutions applied on solid clay bricks substrates. Dry carbon fiber textiles (C) and polymer-coated glass fiber textiles (G), with different hydraulic lime mortar matrices, were tested. Two different bond lengths (150 and 250 mm) were considered, and the exposure temperature levels were 20, 200 and 400 °C. The main conclusions drawn from the study are as follows:

- At 20 °C, the behavior of the TRMs studied depends largely on the bond length adopted, as expected and as reported in other studies. In sufficiently anchored meshes, the failure occurs by tensile rupture of the fibers and the textiles can be practically fully exploited. For insufficient bond lengths, failure occurs by slippage of the fibers with respect to the mortar matrix, and the textiles work at approximately half of their capacity. It can therefore be concluded that it is essential to provide the meshes with a sufficient anchorage length to fully exploit their mechanical capacity.
- At 200 °C all the series studied fail by slippage of the meshes with respect to the mortar matrix, regardless of the bond length adopted. The fundamental difference with respect to the series tested at 20 °C lay in the fact that the fibers cannot fully develop their tensile strength even if they have been properly anchored. The bond between the fabric and the mortar seems to be compromised at this temperature level. However, it should be noted that the TRMs analyzed retain a substantial portion of their bonding capacity at 200 °C, since losses range from 24% (C) to 34% (G).
- The failure mode of TRMs with carbon fibers undergoes a radical change at 400 °C, temperature at which debonding of the mortar matrix from the brick substrate occurs, at very low stresses and regardless of the bond length adopted. Therefore, it can be concluded that the TRM practically loses all its bond capacity under these conditions, probably due to the influence of temperature on the synthetic fibers and polymers in the mortar composition. With respect to the glass fiber meshes, the failure mode is similar to that described for the series exposed to 200 °C. The bond strength loss is of the same order (29%), so that in this case it seems that the TRM is able to retain much of its capacity.
- To prevent debonding failure at the matrix-to-substrate interface as described in the previous point, it could be interesting to explore the possibility of introducing connectors to anchor the TRM to the brick substrate. This aspect is beyond the scope of this paper and is proposed as a possible line of investigation for future studies.

CRediT authorship contribution statement

L. Estevan: Investigation, Methodology, Writing – original draft. **F. J. Baeza:** Conceptualization, Formal analysis, Writing – review & editing. **F.B. Varona:** Investigation, Writing – review & editing, Funding acquisition. **J. Pereiro:** Investigation, Writing – review & editing, Visualization.

Declaration of Competing Interest

The authors declare that they have no known competing financial interests or personal relationships that could have appeared to influence the work reported in this paper.

Data availability

Data will be made available on request.

Acknowledgements

The authors would like to acknowledge Mapei Spain and Grupo Puma for the materials supplied in this work. This research has been funded by the Spanish Ministry of Science, Innovation and Universities, grant number RTI2018-101148-B-100.

References

[1] L.N. Koutas, Z. Tetta, D.A. Bournas, T.C. Triantafillou, Strengthening of concrete structures with textile reinforced mortars: state-of-the-art review, J. Compos. Constr. 23 (2019) 03118001, https://doi.org/10.1061/(asce)cc.1943-5614.0000882.
[2] L.A.S. Kouris, T.C. Triantafillou, State-of-the-art on strengthening of masonry structures with textile reinforced mortar (TRM), Constr. Build. Mater. 188 (2018) 1221–1233, https://doi.org/10.1016/j.conbuildmat.2018.08.039.
[3] C. Papanicolaou, T. Triantafillou, M. Lekka, Externally bonded grids as strengthening and seismic retrofitting materials of masonry panels, Constr. Build. Mater. 25 (2011) 504–514, https://doi.org/10.1016/j.conbuildmat.2010.07.018.
[4] E. Bernat, L. Gil, P. Roca, C. Escrig, Experimental and analytical study of TRM strengthened brickwork walls under eccentric compressive loading, Constr. Build. Mater. 44 (2013) 35–47, https://doi.org/10.1016/j.conbuildmat.2013.03.006.
[5] B. Torres, S. Ivorra, F. Javier Baeza, L. Estevan, B. Varona, Textile reinforced mortars (TRM) for repairing and retrofitting masonry walls subjected to in-plane cyclic loads. an experimental approach, Eng. Struct. 231 (2021), 111742, https://doi.org/10.1016/j.engstruct.2020.111742.
[6] A. Cascardi, F. Micelli, M.A. Aiello, FRCM-confined masonry columns: experimental investigation on the effect of the inorganic matrix properties, Constr. Build. Mater. 186 (2018) 811–825, https://doi.org/10.1016/j.conbuildmat.2018.08.020.
[7] L.N. Koutas, D.A. Bournas, Confinement of masonry columns with textile-reinforced mortar jackets, Constr. Build. Mater. 258 (2020), 120343, https://doi.org/10.1016/j.conbuildmat.2020.120343.
[8] L. Estevan, F.J. Baeza, D. Bru, S. Ivorra, Stone masonry confinement with FRP and FRCM composites, Constr. Build. Mater. 237 (2020), 117612, https://doi.org/10.1016/j.conbuildmat.2019.117612.
[9] V. Alecci, G. Misseri, L. Rovero, G. Stipo, M. De Stefano, L. Feo, R. Luciano, Experimental investigation on masonry arches strengthened with PBO-FRCM composite, Compos. Part B Eng. 100 (2016) 228–239, https://doi.org/10.1016/j.compositesb.2016.05.063.
[10] F.G. Carozzi, C. Poggi, E. Bertolesi, G. Milani, Ancient masonry arches and vaults strengthened with TRM, SRG and FRP composites: experimental evaluation, Compos. Struct. 187 (2018) 466–480, https://doi.org/10.1016/j.compstruct.2017.12.075.
[11] E. Bertolesi, B. Torres, J.M. Adam, P.A. Calderón, J.J. Moragues, Effectiveness of textile reinforced mortar (TRM) materials for the repair of full-scale timbrel masonry cross vaults, Eng. Struct. 220 (2020), 110978, https://doi.org/10.1016/j.engstruct.2020.110978.
[12] S. De Santis, F.G. Carozzi, G. de Felice, C. Poggi, Test methods for textile reinforced mortar systems, Compos. Part B Eng. 127 (2017) 121–132, https://doi.org/10.1016/j.compositesb.2017.03.016.
[13] G. de Felice, M.A. Aiello, C. Caggegi, F. Ceroni, S. De Santis, E. Garbin, N. Gattesco, Ł. Hojdys, P. Krajewski, A. Kwiecień, M. Leone, G.P. Lignola, C. Mazzotti, D. Oliveira, C. Papanicolaou, C. Poggi, T. Triantafillou, M.R. Valluzzi, A. Viskovic, Recommendation of RILEM technical committee 250-csm: test method for textile reinforced mortar to substrate bond characterization, Mater. Struct. Constr. 51 (2018) 1–9, https://doi.org/10.1617/s11527-018-1216-x.
[14] F.G. Carozzi, A. Bellini, T. D'Antino, G. de Felice, F. Focacci, Ł. Hojdys, L. Laghi, E. Lanoye, F. Micelli, M. Panizza, C. Poggi, Experimental investigation of tensile and bond properties of Carbon-FRCM composites for strengthening masonry elements, Compos. Part B Eng. 128 (2017) 100–119, https://doi.org/10.1016/j.compositesb.2017.06.018.
[15] G.P. Lignola, C. Caggegi, F. Ceroni, S. De Santis, P. Krajewski, P.B. Lourenço, M. Morganti, C.(Papanicolaou, C. Pellegrino, A. Prota, L. Zuccarino, Performance assessment of basalt FRCM for retrofit applications on masonry, Compos. Part B Eng. 128 (2017) 1–18.
[16] M. Leone, M.A. Aiello, A. Balsamo, F.G. Carozzi, F. Ceroni, M. Corradi, M. Gams, E. Garbin, N. Gattesco, P. Krajewski, C. Mazzotti, D. Oliveira, C. Papanicolaou, G. Ranocchiai, F. Roscini, D. Saenger, Glass fabric reinforced cementitious matrix: tensile properties and bond performance on masonry substrate, Compos. Part B Eng. 127 (2017) 196–214, https://doi.org/10.1016/j.compositesb.2017.06.028.
[17] A. Bellini, M.A. Aiello, F. Bencardino, C.B. de Carvalho Bello, G. Castori, A. Cecchi, F. Ceroni, M. Corradi, T. D'Antino, S. De Santis, M. Fagone, G. de Felice, M. Leone, G.P. Lignola, A. Napoli, M. Nisticò, C. Poggi, A. Prota, G. Ranocchiai, R. Realfonzo, E. Sacco, C. Mazzotti, Influence of different set-up parameters on the bond behavior of FRCM composites, Constr. Build. Mater. 308 (2021) 124964.
[18] J. Donnini, G. Maracchini, S. Lenci, V. Corinaldesi, E. Quagliarini, TRM reinforced tuff and fired clay brick masonry: experimental and analytical investigation on their in-plane and out-of-plane behavior, Constr. Build. Mater. 272 (2021), 121643, https://doi.org/10.1016/j.conbuildmat.2020.121643.
[19] T. D'Antino, A.S. Calabrese, C. Poggi, Experimental procedures for the mechanical characterization of composite reinforced mortar (CRM) systems for retrofitting of masonry structures, Mater. Struct. Constr. 53 (2020) 1–18, https://doi.org/10.1617/s11527-020-01529-1.
[20] P.D. Askouni, C.G. Papanicolaou, Experimental investigation of bond between glass textile reinforced mortar overlays and masonry: the effect of bond length, Mater. Struct. Constr. 50 (2017) 1–15, https://doi.org/10.1617/s11527-017-1033-7.
[21] P.D. Askouni, C. Corina, G. Papanicolaou, Textile Reinforced Mortar-to-masonry bond: experimental investigation of bond-critical parameters, Constr. Build. Mater. 207 (2019) 535–547, https://doi.org/10.1016/j.conbuildmat.2019.02.102.
[22] P.D. Askouni, C. "Corina" G. Papanicolaou, Role of mortar joints in textile reinforced mortar-to-masonry bond, J. Compos. Constr. 24 (2020) 1–12, https://doi.org/10.1061/(asce)cc.1943-5614.0001056.
[23] X. Wang, C.C. Lam, V.P. Iu, Bond behaviour of steel-TRM composites for strengthening masonry elements: experimental testing and numerical modelling, Constr. Build. Mater. 253 (2020), 119157, https://doi.org/10.1016/j.conbuildmat.2020.119157.
[24] A. Dalalbashi, B. Ghiassi, D.V. Oliveira, A multi-level investigation on the mechanical response of TRM-strengthened masonry, Mater. Struct. Constr. 54 (2021) 1–19, https://doi.org/10.1617/s11527-021-01817-4.
[25] F. Wang, N. Kyriakides, C. Chrysostomou, E. Eleftheriou, R. Votsis, R. Illampas, Experimental research on bond behaviour of fabric reinforced cementitious matrix composites for retrofitting masonry walls, Int. J. Concr. Struct. Mater. 15 (2021) 1–17, https://doi.org/10.1186/s40069-021-00460-1.
[26] Y. Shiping, W. Boxue, Z. Chenxue, L. Shuang, Bond performance between textile reinforced concrete (TRC) and brick masonry under conventional environment, Structures. 36 (2022) 392–403, https://doi.org/10.1016/j.istruc.2021.12.029.
[27] G. Ferrara, C. Caggegi, A. Gabor, E. Martinelli, Experimental study on the adhesion of basalt textile reinforced mortars (trm) to clay brick masonry: the influence of textile density, Fibers. 7 (2019), https://doi.org/10.3390/?b7120103.
[28] G. Misseri, G. Stipo, S. Galassi, L. Rovero, Experimental investigation on the bond behaviour of basalt trm systems-influence of textile configuration and multi-layer application, Key Eng. Mater. 817 KEM (2019) 134–140, https://doi.org/10.4028/www.scientific.net/KEM.817.134.
[29] A. Bellini, S.K. Shahreza, C. Mazzotti, Cyclic bond behavior of FRCM composites applied on masonry substrate, Compos. Part B Eng. 169 (2019) 189–199, https://doi.org/10.1016/j.compositesb.2019.04.009.
[30] A. Dalalbashi, B. Ghiassi, D.V. Oliveira, Freeze-thaw effects on the performance of TRM-strengthened masonry, J. Build. Eng. 59 (2022), 105077, https://doi.org/10.1016/j.jobe.2022.105077.
[31] S. Yin, F. Wang, C. Zhang, S. Liu, Research on the interface bonding performance between FRCM and masonry under salt erosion environment, J. Build. Eng. 46 (2022), 103755, https://doi.org/10.1016/j.jobe.2021.103755.
[32] A. Bilotta, F. Ceroni, G.P. Lignola, A. Prota, Use of DIC technique for investigating the behaviour of FRCM materials for strengthening masonry elements, Compos. Part B Eng. 129 (2017) 251–270, https://doi.org/10.1016/j.compositesb.2017.05.075.
[33] D.M. Linn, D.G. Aggelis, E. Tsangouri, Single-lap shear tests of textile reinforced mortar retrofit systems bonded to masonry: revealing the fracture progress by digital image correlation and acoustic emission, Mater. Struct. Constr. 55 (1) (2022), https://doi.org/10.1617/s11527-021-01850-3.
[34] E. Bertolesi, M. Fagone, T. Rotunno, E. Grande, G. Milani, Experimental characterization of the textile-to-mortar bond through distributed optical sensors, Constr. Build. Mater. 326 (2022), 126640, https://doi.org/10.1016/j.conbuildmat.2022.126640.
[35] CNR-DT 215/2018, Guide for the Design and Construction of Externally Bonded Fibre Reinforced Inorganic Matrix Systems for Strengthening Existing Structures, CNR - Advisory Committee on Technical Recommendations for Construction, Rome, Italy, (2020).
[36] ACI 549.6R-20, Guide to Design and Construction of Externally Bonded Fabric-Reinforced Cementitious Matrix and Steel-Reinforced Grout Systems for Repair and Strengthening of Concrete Structures, American Concrete Institute, ACI Committee 549, (2020).
[37] L. Bisby, Fire Resistance of Textile Fiber Composites Used in Civil Engineering, in: Text. Fibre Compos. Civ. Eng., 2016: pp. 169–185. https://doi.org/10.1016/B978-1-78242-446-8.00008-2.
[38] C.C. Papanicolaou, T. Triantafillou, Performance of TRM/TRC systems under elevated temperatures and fire conditions, Am. Concr. Institute, ACI Spec. Publ. (2021) 32–46.
[39] D.A.S. Rambo, F. de Andrade Silva, R.D. Toledo Filho, O. da Fonseca Martins Gomes, Effect of elevated temperatures on the mechanical behavior of basalt textile reinforced refractory concrete, Mater. Des. 65 (2015) 24–33, https://doi.org/10.1016/j.matdes.2014.08.060.
[40] P. Kapsalis, T. Triantafillou, E. Korda, D. Van Hemelrijck, T. Tysmans, Tensile performance of textile-reinforced concrete after fire exposure: experimental investigation and analytical approach, J. Compos. Constr. 26 (2022) 1–23, https://doi.org/10.1061/(asce)cc.1943-5614.0001162.
[41] L. Estevan, F.B. Varona, F.J. Baeza, B. Torres, D. Bru, Textile reinforced mortars (TRM) tensile behavior after high temperature exposure, Constr. Build. Mater. 328 (2022), 127116, https://doi.org/10.1016/j.conbuildmat.2022.127116.
[42] S.M. Raoof, D.A. Bournas, Bond between TRM versus FRP composites and concrete at high temperatures, Compos. Part B Eng. 127 (2017) 150–165, https://doi.org/10.1016/j.compositesb.2017.05.064.
[43] Z. Wang, J.G. Dai, M. Wang, L. Chen, F. Zhang, Q. Xu, Residual bond strengths of epoxy and cement-bonded CFRP reinforcements to concrete interfaces after elevated temperature exposure, Fire Saf. J. 124 (2021), 103393, https://doi.org/10.1016/j.firesaf.2021.103393.

[44] S.R. Maroudas, C.G. Papanicolaou, Effect of high temperatures on the TRM-to-masonry bond, Key Eng. Mater. 747 KEM (2017) 533–541, https://doi.org/10.4028/www.scientific.net/KEM.747.533.
[45] J. Donnini, F. De Caso y Basalo, V. Corinaldesi, G. Lancioni, A. Nanni, Fabric-reinforced cementitious matrix behavior at high-temperature: Experimental and numerical results, Compos. Part B Eng. 108 (2017) 108–121.
[46] L. Ombres, A. Iorfida, S. Mazzuca, S. Verre, Bond analysis of thermally conditioned FRCM-masonry joints, Meas. J. Int. Meas. Confed. 125 (2018) 509–515, https://doi.org/10.1016/j.measurement.2018.05.021.
[47] A. Iorfida, S. Candamano, F. Crea, L. Ombres, S. Verre, P. De Fazio, Bond behaviour of FRCM composites: effects of high temperature, Key Eng. Mater. 817 KEM (2019) 161–166, https://doi.org/10.4028/www.scientific.net/KEM.817.161.
[48] P.D. Askouni, C.(.G. Papanicolaou, M.I. Kaffetzakis, The effect of elevated temperatures on the TRM-to-masonry bond: comparison of normal weight and lightweight matrices, Appl. Sci. 9 (10) (2019) 2156.
[49] P.D. Askouni, C.(.G. Papanicolaou, L. Azdejkovic, Experimental investigation of the trm-to-masonry bond after exposure to elevated temperatures: cementitious and alkali-activated matrices of various densities, Materials (Basel). 15 (1) (2022) 140.
[50] F. Ferretti, M. Canestri, C. Mazzotti, Effect of temperature variations on the bond behavior of FRCM applied to masonry, Mater. Struct. Constr. 55 (2022) 1–14, https://doi.org/10.1617/s11527-022-02002-x.
[51] L. Estevan, B. Torres, F.B. Varona, F.J. Baeza, S. Ivorra, Shear strengthening of masonry walls with Textile Reinforced Mortars (TRM) under high temperature exposure, J. Build. Eng. 63 (2023), 105511, https://doi.org/10.1016/j.jobe.2022.105511.
[52] UNE-EN 772-1:2011+A1:2016, Methods of test for masonry units - Part 1: Determination of compressive strength, (2016).
[53] UNE-EN 772-6:2002, Methods of test for masonry units - Part 1: Determination of bending tensile strength of aggregate concrete masonry units, (2002).
[54] UNE-EN 1015-11:2020, Methods of test for mortar for masonry - Part 11: Determination of flexural and compressive strength of hardened mortar, (2020).
[55] UNE-EN 1052-1, Methods of test for masonry - Part 1: Determination of compressive strength, (1999).
[56] ASTM D2845–08, Standard Test Method for Laboratory Determination of Pulse Velocities and Ultrasonic Elastic Constants of Rock, ASTM International, West Conshohocken, PA, (2008).